Plasma Immersion Ion Implantation in Radio Frequency Plasma

*B. Bora, H. Bhuyan, E. Wyndham, H. Chuaqui, M. Favre

Department of Physics, Pontificia Universidad Católica de Chile, Ave. Vicuña Mackenna 4860, Santiago,Chile

*Corresponding author e-mail: bbora@fis.puc.cl

Abstract

Plasma immersion ion implantation (PIII) has attracted wide interests since it emulates conventional ion-beam ion implantation (IBII) in niche applications. For instance, the technique has very high throughput, the implantation time is independent of the sample size, and samples with an irregular shape can be implanted without complex beam scanning or sample manipulation. For uniform ion implantation and deposition on to different substrates, like silicon, stainless steel etc., a capacitive coupled Radio frequency (RF), 13.6 MHz, plasma is used. During the PIII process, the physical parameters which are expected to play crucial rule in the deposition process like RF power, Negative pulse voltage and pulse duration, gas type and gas mixture, gas flow rates and the implantation dose are studied. The ion dose is calculated by dynamic sheath model and the plasma parameters are calculated from the V-I characteristic and power balance equation by homogeneous model of rf plasma discharge considering Ohmic as well as Stochastic heating. The correlations between the yield of the implantation process and the physical parameters as well as plasma parameters are discussed.

1. Introduction

Plasma immersion ion implantation (PIII) has been shown to be an effective surface modification and materials fabrication technique [1]. The main motivation for developing this technique is to improve the surface properties of materials [2]. Currently, PIII has extensive applications in industries, such as material surface modification, microelectronics [2-4] and the synthesis of novel materials [5]. PIII is a process in which a target object is immersed in a plasma and a series of high negative voltage pulses (HNVPs) are applied to the target in order to extract ions from the plasma and implant them into the target [6,7]. When a short HNVP is applied, the electrons are expelled away from the target region on a time scale of the electron oscillation period [8]. In contrast, the ions that cannot respond swiftly to the pulse on such a short time scale as the electrons do move away negligibly from their original locations. The large difference in mobility between the electrons and ions leads to the creation of a region of nearly pure ion space charge, i.e. an ion sheath next to the target surface forms [9-11]. Thus, a strong electric field builds up between the sheath boundary and the target surface [4]. The ions are accelerated and implanted into the target on a much longer time scale [3]. In order to maintain a continuous flow of ions, the ion sheath continues to expand while the externally applied pulse is present. The evolution of the sheath is important for surface modifications, and is directly related to the optimization of discharge parameters, such as the plasma density and the duration and waveform of the externally applied pulse [4]. The plasma characteristics in the sheath have an influential role on the current density and the energy distribution of implanted ions, which determine the implantation efficiency. The homogeneity of the implantation process is directly related to the plasma properties. To achieve a homogeneous implantation process, it is necessary to use homogeneous plasma. Capacitivly couple radio frequency (CCRF) discharge is one of the suitable medium for producing homogeneous plasma and implementation of PIII process [12]. As a result of energetic ions, chemically active species, radicals and also energetic neutral species, rf discharges are widely used in etching, deposition and surface treatment, particularly in the semiconductor industry. Although, much processing is done on an empirical basis for a particular device, a full

characterization is desirable for reproducibility, consistency, better understanding the process, and more importantly transformation of process from one device to another. The yield of ion implantation process in PIII strongly depends on the ion density [13]. It is therefore important to investigate the plasma parameters in such discharge. There are several diagnostic techniques employed for the determination of electron density and temperature in dc plasmas which includes Langmuir probe, plasma spectroscopy, microwave and laser interferometries, and Thomson scattering [14-19]. Several different characterization techniques are reported in recent literature to characterize the atmospheric pressure capacitive couple discharge plasma for different experimental parameters [20-23]. The electrical discharge characteristic can be also used to estimate the plasma parameters, which is simpler, easier, quicker and without used of additional equipments [20]. Although the measurements of plasma parameters are crucial for optimization of the PIII, the optimization process itself involves sophisticated material characterization techniques, which need extra efforts and cost. Shou Zhe Li et al [20] estimated the plasma density and plasma parameters from the current-voltage (I-V) and current-power (I-P) characteristic of an atmospheric pressure capacitive couple rf plasma on the basis of homogeneous discharge model. They have estimated the plasma density in α mode of atmospheric pressure capacitive discharge. They assumed the electron density n_e is only proportional to the rms value of the applied current, because electron neutral collisions are much more frequent in atmospheric pressure which makes the drift velocity of the electron independent on the variation of applied electric field [20]. This model can be used to evaluate the plasma parameters in atmospheric pressure capacitive couple rf plasma. However, large range of measurements on discharge characteristics is required to evaluate the plasma parameters. In addition, in low pressure, which is very important in material processing works when the electron neutral collision reduced and the electron gain more energy from the applied electric field by increasing drift velocity, this model cannot be used directly to evaluate the plasma parameters. In low pressure, particularly in mtorr range, the nonlinear plasma series resonance (PSR) effect is also dominant and produces several harmonics to the rf current [32-34], which need to be considered in evaluating the plasma parameters. As the PIII is concern, there are mainly two important mechanism which determined the yield of the implantation process; one is the production of ion dose to the target which determined the characteristics of the implanted ions like ion dose and ion energy and another is the material-ions interaction where the implemented ions react with the target material. Direct measurements of ion dose to the substrate may give the overall idea to optimize the PIII process for a particular device. Theoretical or simulations calculations of the ion dose can be also used to optimize the ion dos characteristics. Several investigation have been reported including the Child-Langmuir law [24-26], plasma fluid model [27, 28], and particle in cell codes [29, 30]. A simple and user friendly one-dimensional analytical model on the basis of dynamic sheath model to effectively predict the effects of processing parameters on the implanted ion dose for planar target was reported and studied in [31]. In their calculations, they have assumed a perfect HNVP of amplitude V_0 and width t_p, but in the real experiment there always have a rise time and fall time of the pulse, which need to be considered while calculating the ion dose.

In this work, we report a PIII optimization process by evaluating the plasma parameters from the electrical discharge characteristics of a CCRF plasma system on the basis of homogeneous discharge model and experimentally investigating the ion dose to the target. We have also calculated the ion dose by dynamic sheath model and correlate the results with the experimentally observed values. To evaluate the plasma parameters the homogeneous discharge model of CCRF is modified to make it applicable for wide range of operating

pressure by adopting the nonlinear PSR effect. In this modified model, it is also considered the drift velocity of the electron is affected by applied electric field in lower pressure.

2. Experimental Details

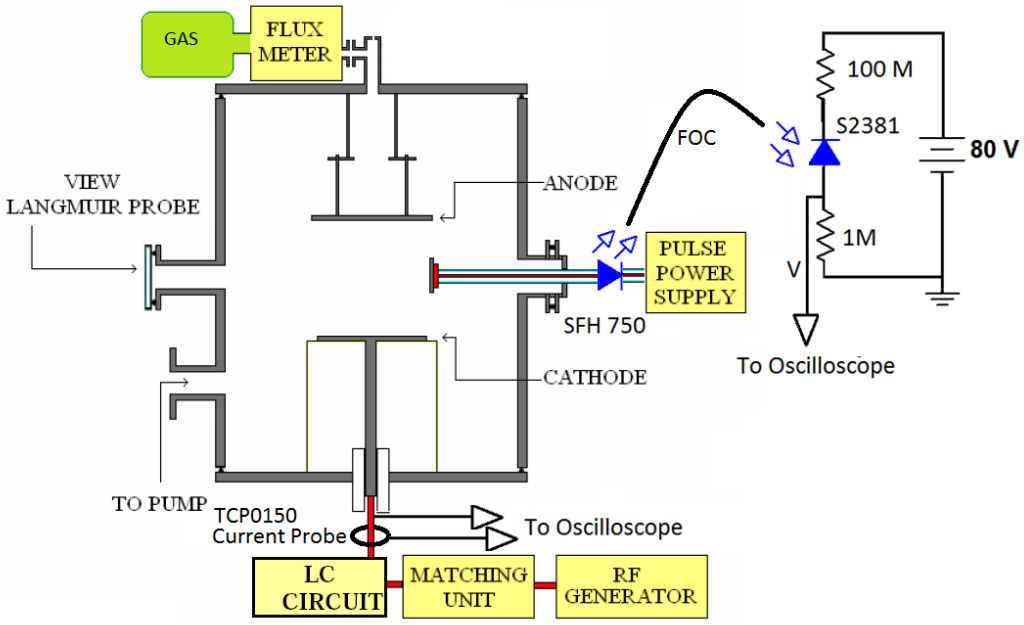

Figure 1. Experimental system.

The experimental set up of the CCRF system is shown in figure 1. The electrode assembly of the rf discharge is consists of two water cooled circular disc shaped parallel stainless steel electrodes separated by 11 cm. The diameter of the lower powered electrode is 8 cm and the upper grounded electrode is 10 cm. The pressure in the stainless steel vacuum chamber was maintained by a combination of rotary and turbo molecular pumps. Series of mass flow controller are also used for maintaining gas flow rates. The substrate is immersed in the plasma and it is biased by a HNVP produced with an in-house developed power supply. To measure the pulse current and properly isolate the biasing circuit an optical isolator is used. A combination of SFH 750 plastic fiber optic transmitter diode and S2381 photodiode along with a fiber optic cable are used as an optical isolator. A voltage probe is used to measure the pulse voltage and it is recorded along with the pulse current in an oscilloscope. The rf discharge current is measured by a Tektronix TCP0150 current probe and the signals are recorded with a Tektronix DPO-4104 oscilloscope for further analysis. An automatic matching network (ENI MWH-5-01) is connected in between the rf power supply and the electrodes to deliver maximum power to the load. The rf power generator (ENI ACG-6B) can deliver up to a maximum of 600W and is equipped with a pair of meters for simultaneously monitoring forward power and reflected power. Electrical signals from the plasma are recorded only when there is no reflected power. Bulk plasma is produced and filled in the space between the electrodes and the electrodes are covered by sheath regions. A negative dc potential develops between the bulk plasma and the power electrodes, which is termed as 'self bias' in rf plasma. This self bias is generated as a consequence of the geometrical asymmetry of the electrode system. Due to this 'self bias' the ion energies near the power electrode

reaches up to few hundred eV. The experimental parameters varied are operating power (10W to 120W) and pressure (10 mtorr to 350 mtorr). The three measured quantities i.e. rms values of current I_{rms}, rms values of voltage V_{rms}, and average power P are used to calculate plasma parameters from modified homogeneous discharge model as describe in the section 3.1. On the other hand, the ion dose are calculated from the pulse current I_p (Section 3.2). The pulse voltage V_p is used to calculate the ion dose from the dynamic sheath model as describe in the section 3.3.

3. Model

3.1. Homogeneous Discharge Model

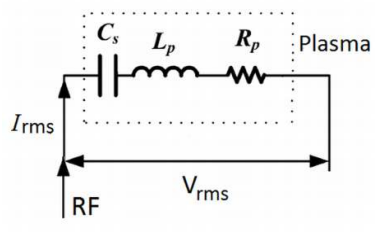

Figure 2. Equivalent circuit of the homogeneous discharge CCRF plasma.

In homogeneous discharge model of CCRF, the plasma is considered as a series of sheath capacitor (C_s), a bulk plasma resistor (R_p), and a bulk plasma inductor (L_p) as shown in figure 2. In the bulk of the plasma, the electron frequency, $\omega_{pe}^2 = n_e^2 / \varepsilon_0 m$ and the capacitance of the parallel electrodes c_0, can be used to express the time average inductance due to the inertia of the bulk plasma electron as follows [20, 32]

$$L_p = \frac{1}{\omega_{pe}^2 c_0} = \frac{md}{An_e e^2} \tag{1}$$

where, m mass of the electron, d distance between the electrodes, A surface area of the parallel plate, n_e electron density. The plasma bulk is assumed to be quasineutral and (for simplicity) homogeneous. The radio frequency current through the discharge is carried by electron conduction alone. The dependence of the current density on the electric field can thus be modelled by a generalized Ohm's law. It takes into account the acceleration of the electrons by the electric field and their momentum loss due to elastic collisions with the neutrals of the background gas. By considering the ohmic and stochastic heating, the resistance of the plasma bulk R_p can be expressed as [20, 32],

$$R_p = \frac{(\nu_m + v_e / l_p) L_p}{c_f} \tag{2}$$

where, ν_m and v_e are the electron neutral collision frequency and the mean thermal speed, respectively. c_f is a correction factor introduced to the plasma resistance due to the change in drift velocity of the electrons with the variation of the electric field and also for the PSR effect. Since the electrons have sufficient distance to travel and accelerate in the bulk plasma at low pressure, we anticipate that the resistance of the bulk plasma changes due to the change in drift velocity of the electrons depending on the electric field and pressure. Besides, it was reported that due to the PSR effect the measured rms current is higher than the current predicted by homogeneous discharge model [33, 34]. It has also been experimentally observed that at the beginning of the rf cycle the plasma sheath expands and as a result energetic electron beams are generated [35, 36]. The PSR effect enhances the generation of

these highly energetic electron beams due to the rapid expansion of the sheath. These electrons travel from the sheath region and propagate through the bulk plasma and enhance the total plasma current.

In terms of electron density and electron temperature the equation (2) becomes [21, 34],

$$R_p = \frac{dd_{col}^2}{Ae^2 c_f}\left(8m\pi kT_e\right)^{1/2}\left(1+\frac{(e/k)^2}{\pi d_{col}^2}\frac{1}{n_e}\right) \tag{3}$$

Where, d_{col} is the electron neutral collision cross section and T_e is the electron temperature. In homogenous model, the sheath capacitance can be expressed as [20, 32]

$$C_S = \frac{en\omega\varepsilon_0 A^2}{2I_p} \tag{4}$$

Where, ω is the applied rf frequency. The rms values of current *(I_{rms})* and voltage *(V_{rms})* according to the equivalent circuit (figure 2) can now be expressed as,

$$V_{rms}^2 = I_{rms}^2\left[8m\pi k\frac{1}{c_f^2}\left(\frac{dd_{col}^2}{Ae^2}\right)^2 T_e\left(1+\frac{(e/k)^2}{\pi d_{col}^2}\frac{1}{n_e}\right)^{1/2}+\left(\frac{md\omega}{Ae^2}-\frac{2}{e\varepsilon_0\omega^2A^2}I_{rms}\right)^2\frac{1}{n_e^2}\right] \tag{5}$$

Li *et al* [20] shows that for atmospheric pressure CCRF plasma the rms value of voltage follows the variation of the rms value of current according to one branch of hyperbola. This is a special case of the equation (5), when the drift velocity of the electrons in the plasma bulk depends trivially on the variation of electric field due to frequent electron-neutral collision and the PSR effect is negligible. The average dissipated power in the plasma and the rms values of current and voltage can be correlated in terms of power factor as,

$$P = V_{rms} I_{rms} \cos\phi \tag{6}$$

Where, ϕ is the phase difference, the equation (6) can be expressed from the equivalent circuit as

$$\cos^{-1}\left(\frac{P}{V_{rms}I_{rms}}\right) = \tan^{-1}\left[\frac{m\omega c_f}{(8m\pi k)^{1/2}d_{col}^2}\left(1+\frac{(e/k)^2}{\pi d_{col}^2}\frac{1}{n_e}\right)^{-1}\left(1-\frac{2e}{\varepsilon_0\omega^3 Amd}I_{rms}\right)\frac{1}{n_e}T_e^{-1/2}\right] \tag{7}$$

The power density *p (W/cm^3)* of the plasma can be expressed in terms of temperature and density as power balance equation [20, 37],

$$p = n_e n_g K_{iz}\varepsilon_{iz} + n_e n_g K_{ex}\varepsilon_{a^*} + n_e n_g K_{el,e-a}\frac{3m}{M}T_e \tag{8}$$

The temperature dependent terms K_{iz}, K_{ex} and $K_{el, e\text{-}a}$ along with other terms in equation (8) are well describe in reference [20, 32, 38]. The equations (5), (7) and (8) were solved simultaneously to determine the plasma temperature T_e, plasma density n_e and the correction factor c_f.

3.2. Calculation of Ion Dose

Due to the application of HNVP, an ion matrix sheath is formed and the current to the substrate is completely due the ion, and hence the total current to the substrate per pulse can be obtained by integrating the measured pulse current over the time,

$$\textbf{Ion dos} = \int_0^{\infty} I_p dt \tag{9}$$

3.3 Dynamic Sheath Model

The sheath voltage is always greater than the electron temperature, thus a quasi-static Child–Langmuir law sheath exists at all time and the ion current is spatially constant within the sheath. The implantation ion current J_i , can thus be described using the Child–Langmuir law. For a voltage V_a across a collisionless sheath of thickness S, the ion current is [31]

$$J_i = \frac{4}{9}\varepsilon_0 \left(\frac{2q}{M}\right)^{1/2} \frac{V_a^{3/2}}{S^2} \tag{10}$$

Where ε_0 *is the free-space permittivity,* q *is the ion* charge, and M *is the ion mass.*
In the dynamic sheath model, it is assumed that the ion current, J_i , arises from the ions within the moving sheath, therefore,

$$J_i = q n_e \frac{dS}{dt} \tag{11}$$

Where, n_0 is the plasma density. Equating above two equations and integrating over time, the ion dos can be express as,

$$\text{Ion dos} = n_e S = n_e \left[\left(\frac{4\varepsilon_0}{3qn_0}\right)\left(\frac{2q}{M}\right)^{\frac{1}{2}} \int V_a^{\frac{3}{2}} dt\right]^{\frac{1}{3}} \tag{13}$$

4. Result and Discussions

A typical 3-D surface plot of the current waveforms for different operational rf power at a constant operating pressure of 15 mtorr pressureare shown in figure 3 (a). This figure clearly shows the distortion in current waveforms due to the PSR effect for entire range of the rf power. The recorded current waveforms for different operational pressure at 50 watt rf power are shown in figure 3(b). The distortions on the current waveforms are reduced with increase in pressure. Similar observations are also observed from the Fast Fourier Transformation (FFT) of these current waveforms as shown in the figure 4(a) and figure 4(b) respectively. From these figures it is observed that the change in rf power only changes the amplitude of the current waveforms and the Fourier components. These Fourier transformations show up to

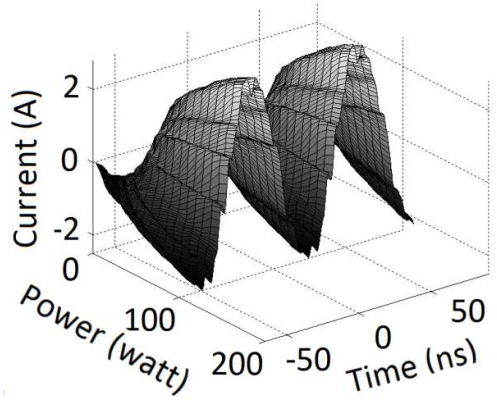

(a)

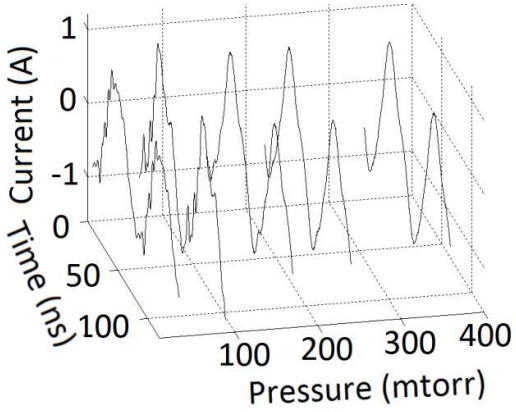

(b)

Figure 3. Current waveforms recorded (a) at 15 mtorr pressure for different rf power and, (b) at 50 watt rf power for different pressure.

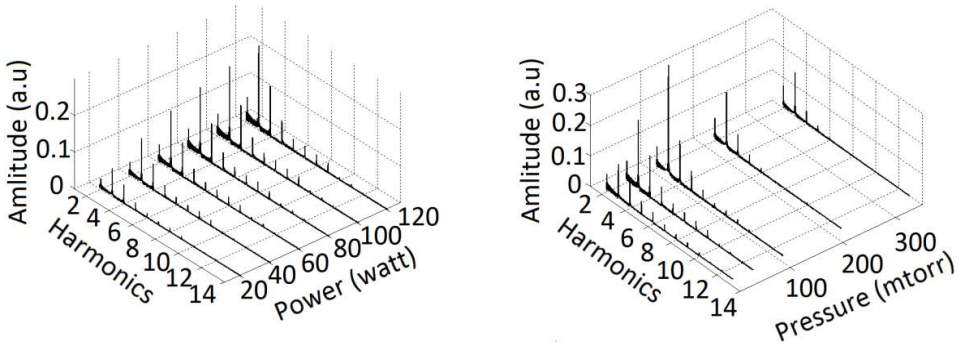

Figure 4. Fourier transformation of the current waveforms recorded (a) at 15 mtorr pressure for different rf power and (b) at 50 watt rf power for different pressure.

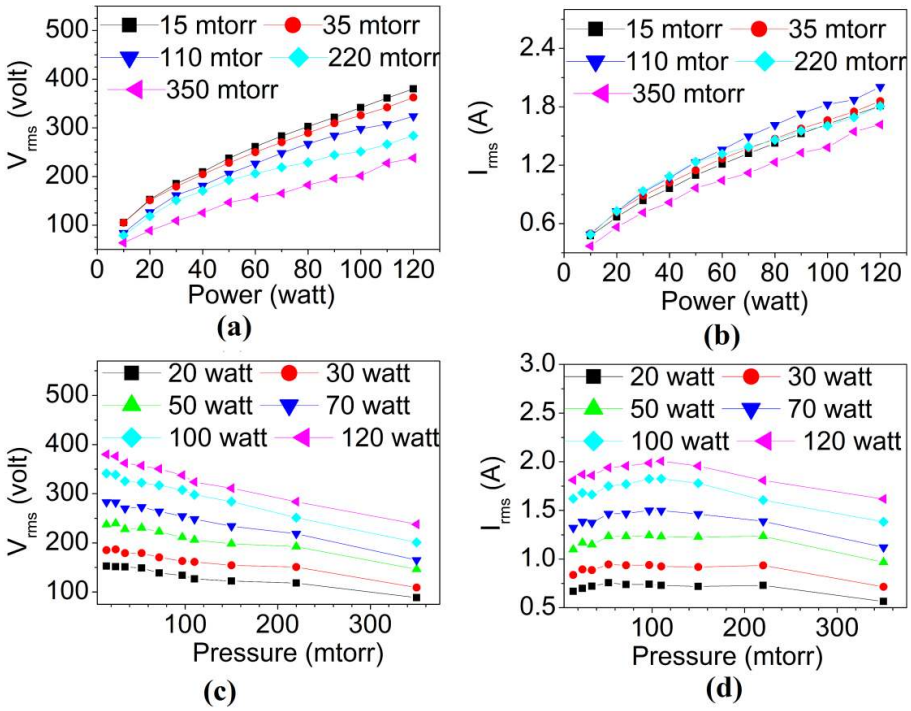

Figure 5. Variation of measured values of rms current and rms voltage with (a),(b) rf power and (c),(d) pressure.

10th harmonics of the applied frequency. The PSR effect is found to reduce with increasing pressure as the high order harmonics are seen to get diminished. The measured I_{rms} and V_{rms} for different rf power and operating pressure are shown in figure 5. The calculated current density is in the range of 4.7 mA/cm^{-2} to 25.5 mA/cm^{-2}. Figure 6(a) shows the V_{rms}–I_{rms} characteristic in the present experimental range and it is look like almost linear. However a small variation in total plasma impedance with increasing rf power for entire experimental range is observed. At higher pressure (350 mtorr), the impedance increases rapidly with decreasing rf power in lower rf power range whereas the impedance decreases with

decreasing rf power at lower pressure. The computational results obtain for electron density and electron temperature for different rf power and operating pressure are shown in figure 7. The electron density are found to be in the range of $0.5x10^{10}$ cm^{-3} to $4x10^{10}$ cm^{-3}, and the

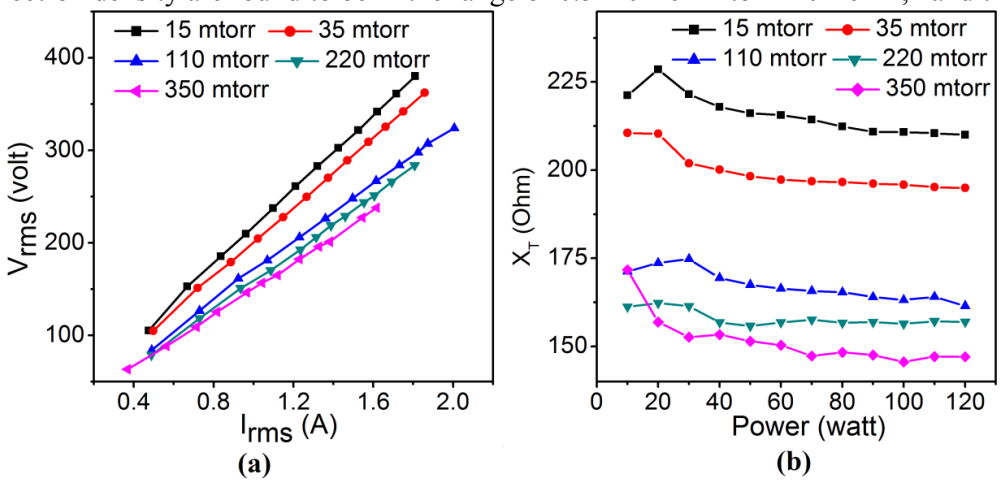

Figure 6.(a) I_{rms}-V_{rms} characteristic of the CCRF discharge at different operating pressure, (b)variation of the total plasma impedance with rf power.

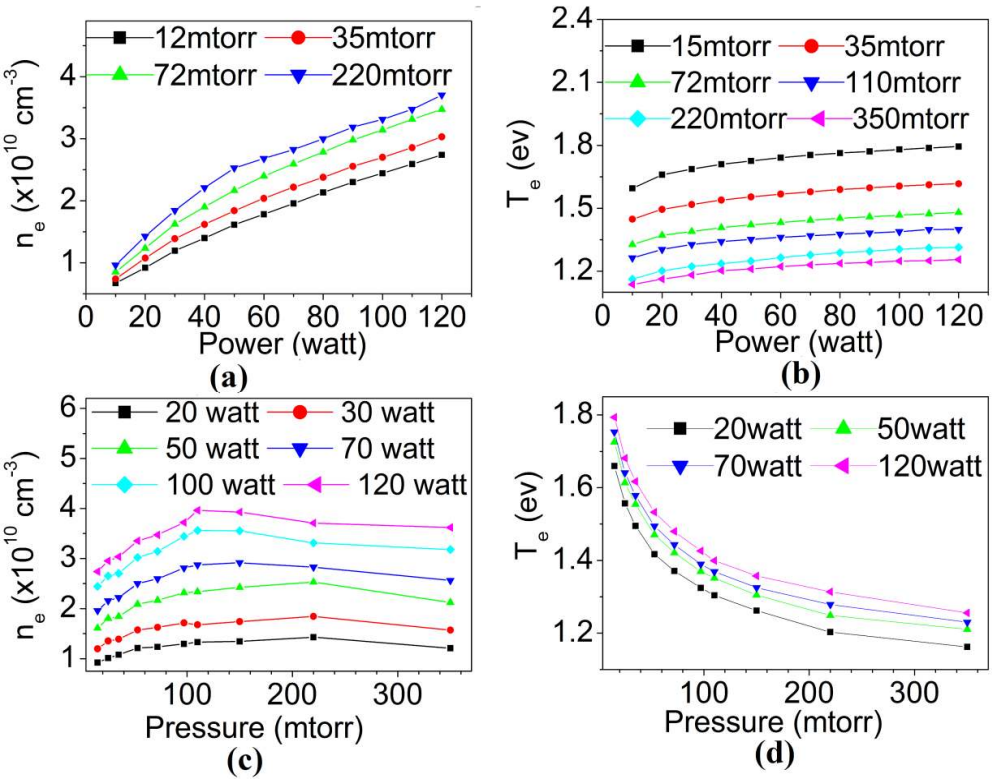

Figure 7. Variation of electron density and temperature(a),(b) with power in different pressure, (c),(d) with pressure in different power respectively.

electron temperature in between 1.4 ev to 1.63 ev, which is well agree with the reported rf compensated Langmuir probe measurement data with the same experimental conditions[12]. Both the electron temperature and density is observed to increase with increasing rf power for the entire operational pressure range. The electron density is initially increasing with

increasing operating pressure and then decreases slowly with further increase in operational pressure. This non-linear variation of electron density with the operational pressure may be due to the existence of the PSR effect in low pressure.

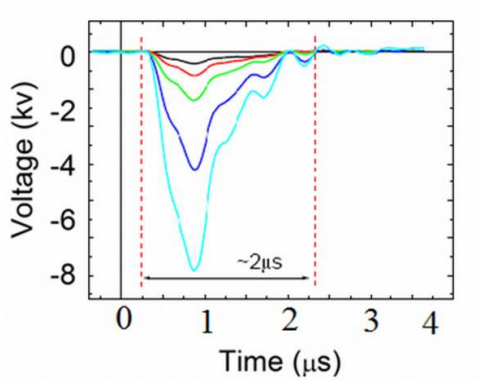

Figure 8. Typical HVNP applied to the target during PIII.

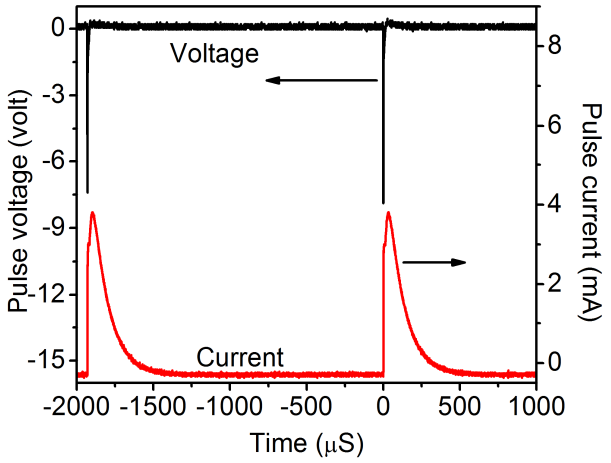

Figure 9. Typical pulse current recorded by optical coupler and HVNP applied to the target during PIII

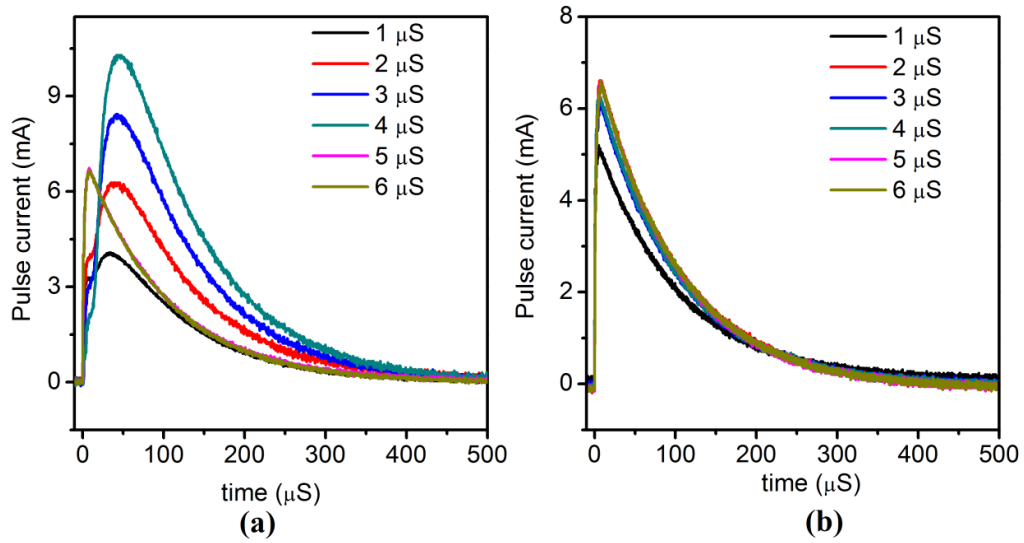

Figure 10. Time evolution of the pulse current for different width of the HVNP at 8 kV pulse voltage, (a) 0.5 kHz, (b) 1 kHz pulse frequency.

The typical HNVP applied to the substrate is shown in the figure 8. Even though the pulse width of the HNVP is few microsecond, the pulse current continues for few hundred microsecond as shown in the figure 9. This is because of the formation of the ion matrix sheath. Significance differences in the pulse current are observe for different pulse voltage, pulse width and pulse frequency. Typical pulse current for different pulse width of the HNVP at 8 kV pulse voltage for 0.5 kHz and 1 kHz are shown in the figure 10. For the pulse

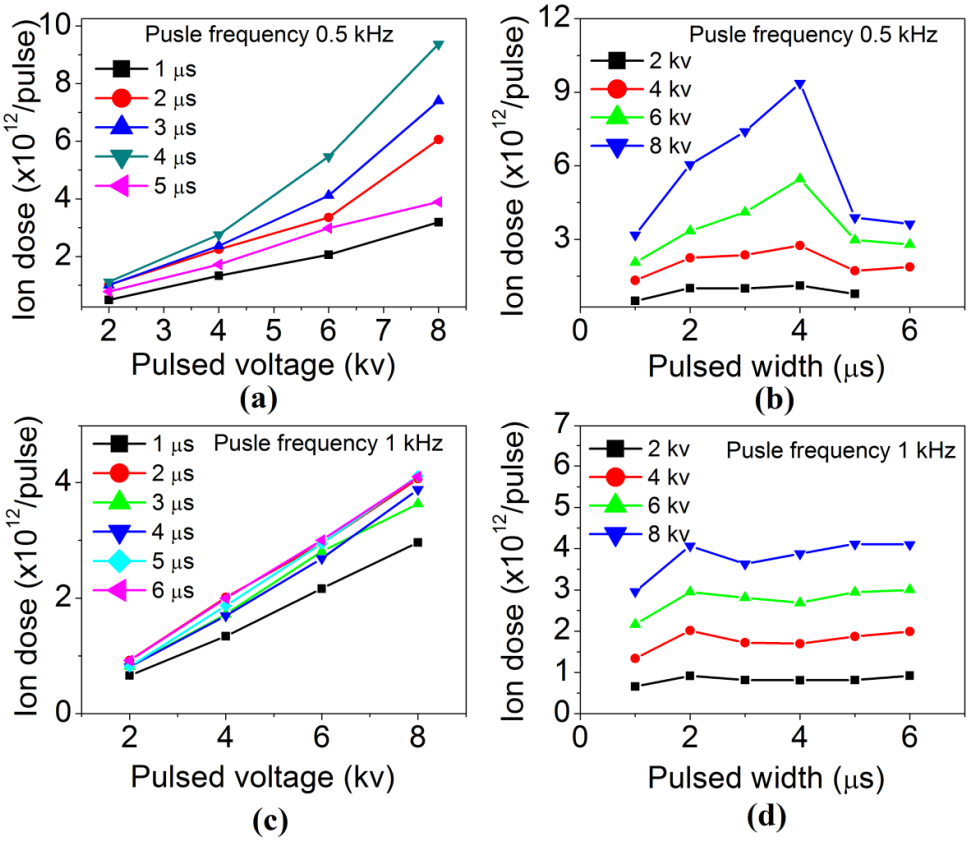

Figure 11. Variation of the ion dos to the target with the pulse voltage and pulse width (a), (b) for 0.5 kHz frequency and (c), (d) for 1 kHz frequency respectively.

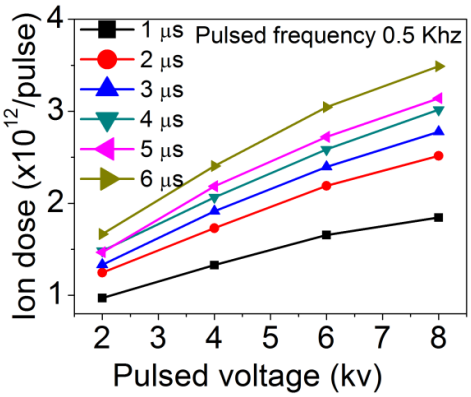

Figure12. Ion dose calculated from the dynamic sheath model and its variation with pulse voltage for different pulse width at 0.5 kHz frequency.

frequency of 0.5 kHz, a sharp delay is observed in rising of the pulse current, whereas no such type of delay is observed for 1 kHz. The calculated ion dose to the substrate and its variation with the pulse voltage and the pulse width of the HVNP for 0.5 kHz and 1 kHz pulse frequency are shown in the figure 11. The ion dos is found to increase almost linearly with pulse voltage for 1 kHz pulse frequency, but for the 0.5 kHz frequency the ion dos is increase more rapidly with pulse voltage.

The calculated ion doses from the dynamic sheath model for different pulse width and pulse voltage at 0.5 kHz frequency are shown in figure 12. The variation of the calculated ion dose with pulse voltage on the basis of the dynamics sheath model shows almost similar trend with experimentally observed one.

5. Conclusion

A study on the CCRF system for PIII process is carried out. The electrical discharge characteristic are analyzed and found several order of harmonics, which lead to increase the heating of the plasma. The homogeneous discharge model of CCRF plasma has been modified by incorporating the PSR effect and this modified model is used to evaluate the plasma parameters. The ion dose to the substrate during the PIII is measured and the results are compared with the dynamics sheath model.

Acknowledgments

The authors acknowledge the support of the FONDECYT 3110008 and Proyecto Puente VRI N° 06/2011 in undertaking this work.

References

1. J.R. Conrad, J.L. Radtke, R.A. Dodd, F.J.Worzala, N.C. Tran, *J. Appl. Phys.* 2 (1987) 4951.
2. M. Shamim, J.T. Scheuer and J.R. Conrad J R, *J. Appl. Phys.* **69 (**1991) 2904.
3. M. Bilek, *J. Appl. Phys.* **89 (**2001) 923.

4. T.K. Kwod, X.C. Zeng, C. Chan and P.K. Chu, *J. Appl. Phys.* **87 (**2000) 4094.
5. P.K. Chu and C. Chan, *Surf. Coat. Technol.* **136 (**2001)151.
6. V. Vahedi, M.A. Lieberman, M.V. Alves, J.P. Verboncoeur and C.K. Birdsall, *J. Appl. Phys.* **69 (**1991)2008.
7. D.Z. Wang, *J. Appl. Phys.* **85(**1999) 3949.
8. J.R. Conrad, J.L. Radtke J L, R.A. Dodd, F.J. Worzala and N.C. Tran, *J. Appl. Phys.* **62 (**1987) 4591.
9. P.K. Chu, S. Qin, C. Chan, N WCheung and L.A. Larson, *Mater. Sci. Eng.* R **17 (**1996) 207.
10. J. Brutscher, R. G¨unzel and W. M¨oller, *Plasma Sources. Sci. Technol.* **5 (**1996)54.
11. S. M¨andl, Brutscher, R. G¨unzel and W. M¨oller *J. Vac. Sci. Technol.* B **14 (**1996) 2701.
12. E. Valderrama, M. Favre, H. Bhuyan, H.M. Ruiz, E. Wyndham, J. Valenzuela, H. Chuaqui, *Surface & Coatings Technology* **204** (2010) 2940.
13. S.M. Chen, R.M. Gwilliam and B.J. Sealy, *Radiation Effects and Defects in Solids* **141** (1997) 149.
14. R. H. Huddlestone and S. L. Leonard, *Plasma Diagnostic Techniques*, London: Academic, 1965.
15. B. Bora, M. Kakati, A.K. Das, *J. Plasma Physics***76** (2010) 699.
16. H. R. Griem, Plasma Spectroscopy McGraw-Hill, New York, 1964.
17. M. A. Heald and C. B. Wharton, *Plasma Diagnostic with Microwaves*, New York: Wiley, 1965.
18. M. C. M. Van de Sanden, J. M. de Regt, G. M. Janssen, J. A. M. Van der Mullen, D. C. Schram, and B. Van der Sijde, *Rev. Sci. Instrum*. **63**(1992) 3369.
19. S. B. Cameron, M. D. Tracy, and J. P. Camaco, *IEEE Trans. Plasma Sci.* **24** (1996) 45.
20. S. Z. Li, J.P. Lim, H. S. Uhm, *Physics Letters A*, **360** (2006).
21. Y.T.Zhang, Q.Q.Li, J.Lou and Q.M. Li *Applied Physics Letters* **97 (**2010) 141504.
22. J.L.Walsh, F. Iza and M.G.Kong, *Applied Physics Letters* **93** (2008) 251502.
23. J.L. Walsh, Y.T.Zhang, F. Iza and M.G. Kong, *Applied Physics Letters* **93** (2008) 221505.
24. M.A. Lieberman, *J. Appl. Phys.* **66** (1989) 2926.
25. P.K. Chu, S. Qin, C. Chan, N.W. Cheung, L.A. Larson, *Mater. Sci. Eng. Reports* **17 (6–7)** (1996) 207.
26. S. Qin, C. Chan, Z. Jin, *J. Appl. Phys.* **79** (1996) 3432.
27. G.A. Emmert, M.A. Henry, *J. Appl. Phys.* **71** (1992) 113.
28. X. B. Tian, D. T. K. Kwok, and Paul. K. Chu, *J. Appl. Phys.* **88** (2000) 4961.
29. T.E. Sheridan, T.K. Kwok, P.K. Chu, *Appl. Phys. Lett.* **72** (1998) 826.
30. D.T.K. Kwok, P.K. Chu, B.P.Wood, C. Chan, *J. Appl. Phys*. **86** (1999) 1817.
31. X. Tian, P. K. Chu, *Physics Letters A* **277** (2000) 42.
32. M.A. Liebermann and A.J. Lichtenberg, *Principles of Plasma Discharges and Materials Processing*, New York: Wiley, 1994.
33. M.A. Lieberman, A.J. Lichtenberg, E. Kawamura, T. Mussenbrock and R.P. Brinkmann, *Physics of Plasmas* **15** (2008) 063505.
34. T. Mussenbrock, R.P. Brinkmann, M.A. Lieberman, A.J. Lichtenberg and E. Kawamura, *Physical Review Letters* 101 (2008) 085004.
35. J. Schulze J, B.G. Heil, D. Luggenholscher, T. Mussenbrock, R.P. Brinkmann and Y. Czarnetzki U *J. Phys. D: Appl. Phys.* **41 (**2008) 42003 .
36. Z. Donkó, J. Schulze, U. Czarnetzki and D. Luggenhölscher, *Appl. Phys. Lett.* **94** (2009) 131501.
37. C. Diplasu, A. Surmeian, A. Groza and M. Ganciu, *Surf. & Coat. Technol.* **203** (2009) 2858.
38. M. Mitchner and J.C.H Kruger, *Partially Ionized Gases,* New York: Wiley, 1973.